

Mechanistic Studies of Highly Enantio- and Diastereoselective Aza-Petasis–Ferrier Rearrangement Catalyzed by Chiral Phosphoric Acid

Masahiro Terada,^{*,†,‡} Takazumi Komuro,[†] Yasunori Toda,^{†,⊥} and Toshinobu Korenaga[§]

[†]Department of Chemistry, Graduate School of Science, Tohoku University, Aoba-ku, Sendai 980-8578, Japan

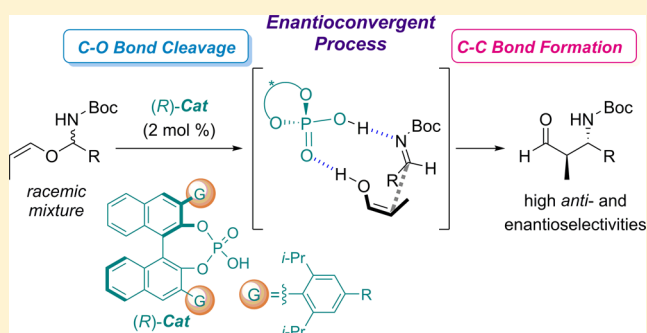
[‡]Research and Analytical Center for Giant Molecules, Graduate School of Science, Tohoku University, Aoba-ku, Sendai 980-8578, Japan

[§]Department of Chemistry and Bioengineering, Graduate School of Engineering, Iwate University, 4-3-5 Ueda, Morioka, Iwate-ken 020-8551, Japan

S Supporting Information

ABSTRACT: The precise mechanism of the highly *anti*- and enantioselective aza-Petasis–Ferrier (APF) rearrangement of hemiaminal vinyl ethers catalyzed by a chiral phosphoric acid was investigated by undertaking experimental and theoretical studies. The APF rearrangement is characterized by the following unique mechanistic features: (i) efficient optical kinetic resolution of the starting racemic hemiaminal vinyl ether, (ii) enantioconvergent process from racemic hemiaminal vinyl ethers to optically active β -amino aldehyde products, and (iii) anomalous temperature effects on the enantioselectivity (enantioselectivity increases as reaction temperature increases). The following experiments were conducted to elucidate the

unique mechanistic features as well as to uncover the overall scheme of the present rearrangement: (A) X-ray crystallographic analysis of the recovered hemiaminal vinyl ether to determine its absolute configuration, (B) rearrangements of enantiomerically pure hemiaminal vinyl ethers to validate the stereochemical relationship between the hemiaminal vinyl ethers and β -amino aldehydes, (C) theoretical studies on the transition states of the C–O bond cleavage and C–C bond formation steps to gain an insight into the optical kinetic resolution of the hemiaminal vinyl ether and the origin of the stereoselectivity, as well as to elucidate the overall scheme of the present rearrangement, and (D) crossover experiments of two hemiaminal vinyl ethers having different vinyl ether and aliphatic substituents to comprehend the mechanism of the anomalous temperature effect and the enantioconvergent process. The results of experiments and theoretical studies fully support the proposed mechanism of the present *anti*- and enantioselective APF rearrangement.



INTRODUCTION

Optically active β -amino carbonyl compounds are highly attractive chiral building blocks for biologically active natural products and synthetic pharmaceutical agents.¹ Among the β -amino carbonyl compounds, β -amino aldehydes represent an important subclass of compounds as they are useful and versatile precursors of γ -amino alcohols, amino acids, β -lactams, and amino sugars. Considerable effort has been devoted to the development of efficient methods for the synthesis of β -amino aldehydes, particularly α -branched aldehydes, in a highly diastereo- and enantioselective manner.

The asymmetric Mannich reaction is the most powerful and efficient method for synthesizing optically active β -amino aldehydes.² In the course of the development of the asymmetric Mannich reaction, a number of efficient approaches that use chiral metal catalysts have been established. Meanwhile, in the past decade, a large number of chiral secondary amine catalysts, such as proline and its derivatives, have emerged as a powerful tool to accelerate the Mannich reaction of *N*-protected aldimines with aldehydes to afford β -amino aldehydes with

high diastereo- and enantioselectivities. At the beginning of the research, *N*-*p*-methoxyphenyl (PMP)-protected imines were widely employed as the electrophilic component.^{3,4} However, strong oxidizing agents were usually required to remove the PMP group on the nitrogen atom of the Mannich products. Hence, the development of a Mannich reaction of aldimines having a readily removable protective group was highly awaited to enhance the synthetic utility of the organocatalytic Mannich reactions. In 2007, the research groups of List⁵ and Cordova⁶ independently reported the proline-catalyzed *syn*-selective direct asymmetric Mannich reaction of aldehydes and imines protected with a readily removable *tert*-butoxycarbonyl (Boc) group. Motivated by those successes, excellent enantioselective methods that use aldimines possessing readily removable protective groups, such as *N*-Boc or *N*-acyl derivatives,⁷ emerged, including *anti*-selective direct asymmetric Mannich reactions.

Received: February 22, 2014

Published: April 18, 2014

However, one critical drawback inherent in the methodologies reported to date is that aromatic or glyoxylate-derived aldimines are employed as adaptive substrates in most cases.^{7c} The enantioselective direct Mannich reaction of aliphatic aldimines has remained largely unexploited because those aldimines readily isomerize to their enamine forms, in particular, *N*-Boc- or *N*-acyl-protected aldimines having proton(s) at the α -position. To overcome this intrinsic problem, we have developed an alternative strategy that involves a combination of two catalytic reactions to furnish optically active β -amino aldehydes having an aliphatic substituent (R) at the β -position, (Figure 1).⁸ The sequence involves an initial metal-catalyzed isomerization of a double bond followed by a chiral Brønsted acid-catalyzed aza-Petasis–Ferrier (APF) rearrangement⁹ using readily available allyl hemiaminal ethers as the substrate.

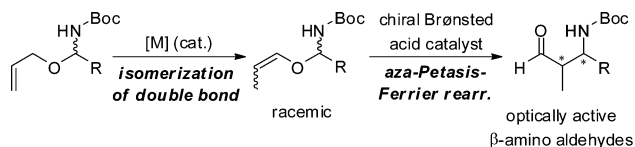


Figure 1. Catalytic sequence for providing optically active β -amino aldehydes having an alkyl substituent at the β -position.

The APF rearrangement proceeds through C–O bond cleavage of the hemiaminal ether moiety by an acid catalyst.¹⁰ Subsequent recombination with C–C bond formation between an imine intermediate and an enol form of the aldehyde results in rearranged products, β -amino aldehydes.^{11–15} In 1993, Frauenrath and co-workers pioneered the diastereoselective APF rearrangement of hemiaminal vinyl ethers promoted by a substoichiometric amount of TMSOTf, an achiral Lewis acid.¹² After that initial report, however, no report by other researchers followed until 2008,¹³ despite the wide applicability of β -amino aldehyde products to the synthesis of a diverse array of nitrogen-containing compounds. Fifteen years after the first discovery, Tayama and co-workers reported a regioselective APF rearrangement of hemiaminal dieny ethers under the influence of a catalytic amount of pyridinium *p*-toluenesulfonate (PPTS), an achiral Brønsted acid.¹⁴ In 2010, Chmielewski and co-workers reported a diastereofacial selective APF rearrangement of the β -lactam framework using chiral 4-vinyl- β -lactam as the substrate and a catalytic amount of Brønsted acid.¹⁵ To the best of our knowledge, there is no report that describes enantioselective catalysis in the APF rearrangement even when chiral metal complexes are taken into consideration, with the exception of our initial report in 2009.⁸

At the beginning of this article, we briefly survey our previous studies on the enantio- and diastereoselective APF rearrangement of hemiaminal vinyl ethers **1**, where the highly stereoselective synthesis of β -amino aldehydes **2** having an aliphatic substituent (R) at the β -position was accomplished using chiral phosphoric acid **3**^{16,17} as the chiral Brønsted acid catalyst¹⁸ (Figure 2). In the established catalytic system, the racemic mixture of hemiaminal vinyl ethers **1** is efficiently converted into enantioenriched β -amino aldehydes **2** through an enantioconvergent process^{19,20} mediated by **3**. Herein, we report in detail mechanistic investigations of the present highly intriguing enantioconvergent process as well as a rationale for the stereochemical outcome on the basis of theoretical studies

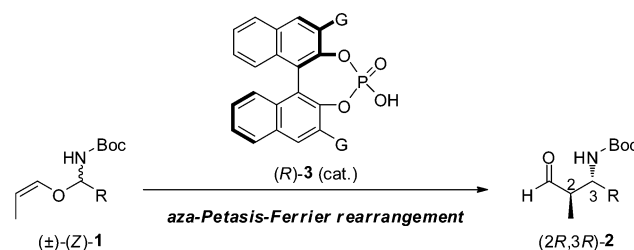


Figure 2. Enantio- and diastereoselective APF rearrangement catalyzed by chiral phosphoric acid.

of the transition states involved in this fascinating 1,3-rearrangement.

RESULTS AND DISCUSSION

Survey of Preliminary Results of Enantio- and Diastereoselective Aza-Petasis–Ferrier Rearrangement and Addressing Issues To Be Clarified.

In our preliminary communication,⁸ we demonstrated the sequential transformation of racemic allyl hemiaminal ethers into optically active β -amino- β -alkyl aldehydes **2** via intermediary vinyl ethers **1** by a combination of two catalytic reactions, as shown in Figure 1. The latter step, APF rearrangement mediated by chiral phosphoric acid **3**, is essential for the enantio- and diastereoselective synthesis of **2** (Figure 3). The enantioselective rearrangement catalyzed by (*R*)-**3** proceeds through the stereoablative loss¹⁹ of a vinyloxy group from the racemic mixture of hemiaminal **1** to generate achiral intermediates, aliphatic aldimine and enol form of the aldehyde, followed by bond recombination through the Mannich-type reaction to form the C–C bond and the generation of two new stereogenic centers at the α - and β -positions under the influence of chiral phosphoric acid catalyst **3**.

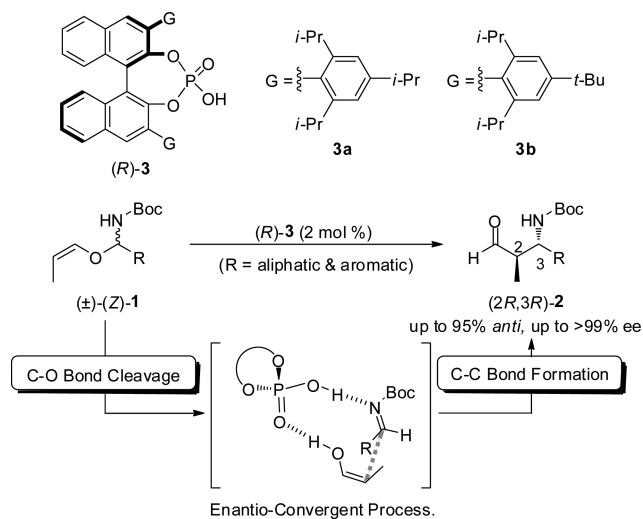
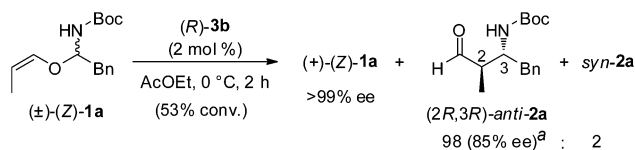


Figure 3. Plausible reaction pathway of the enantioconvergent process.

A thorough screening of several parameters of the present rearrangement, including the geometry of the vinyl subunit, the reaction solvents, the substituent of catalyst **3**, and the reaction temperature, enabled us to establish a highly *anti*- and enantioselective rearrangement. The features of the present catalytic rearrangement are summarized as follows:

- (i) The geometrical purity of **1** affects not only *anti*-selectivity but also enantioselectivity. The use of vinyl ether bearing (*Z*)-geometry is the key structural factor to achieving a highly diastereo- and enantioselective formation of *anti*- β -amino- β -alkyl aldehydes **2**. In contrast, the reaction of the (*E*)-isomer resulted in the alternative *syn*-isomer as the major product albeit with lower diastereo- and enantioselectivities.
- (ii) The solvents used markedly affected the enantioselectivity, whereas high *anti*-selectivity was maintained. Among the solvents examined, relatively basic solvents, such as ethyl acetate and acetone, were the best in terms of chemical yield and enantioselectivity.
- (iii) Chiral phosphoric acids **3a** and **3b** having an isopropyl group and a *tert*-butyl group, respectively, at the 4-position of the phenyl ring had a beneficial effect on the enantioselectivity, although **3b** resulted in a slightly higher enantioselectivity of the product than **3a**.
- (iv) An anomalous temperature effect was observed; a higher temperature resulted in a higher enantioselectivity despite the fact that in a typical enantioselective reaction, the enantioselectivities of the products increase with decreasing reaction temperature.
- (v) Efficient optical kinetic resolution of racemic (*Z*)-**1a** by (*R*)-**3b** was observed at the C–O bond cleavage step (Scheme 1).²¹ (+)-(*Z*)-**1a** was recovered in an enantiomerically pure form at 0 °C, even with approximately 50% conversion of racemic (\pm)-(*Z*)-**1a**. Thus, (–)-(*Z*)-**1a** was consumed much more rapidly than (+)-(*Z*)-**1a** by (*R*)-**3b**, indicating that chiral phosphoric acid (*R*)-**3b** functioned as an efficient resolving catalyst of (\pm)-(*Z*)-**1a**, although the absolute configuration of recovered **1a** had not been determined in our preliminary studies.

Scheme 1. Optical Kinetic Resolution of Racemic Hemiaminal Vinyl Ether (\pm)-(*Z*)-**1a** by Chiral Phosphoric Acid Catalyst (*R*)-**3b**



^aThe % ee of **2a** was determined after reduction of formyl group to alcohol.

As mentioned at the beginning of this section, a sequential protocol that combines the two catalytic reactions and abolishes the need to separate the geometrical isomers of **1** was also demonstrated in our preliminary studies. In order to establish the sequential protocol, we first developed a (*Z*)-selective double bond isomerization of allyl hemiaminal ether **4** using a NiI₂ complex having a bidentate phosphine ligand, dppf, or *p*-tolbiphep.^{8,13,22} The combination of the developed (*Z*)-selective isomerization with an enantioselective APF rearrangement allowed us to accomplish the sequential transformation that does not require the separation of the geometrical isomers of **1**. The present sequential protocol is applicable to a variety of allyl hemiaminal ethers **4** to afford corresponding β -amino- β -alkyl aldehydes **2** in good yields. Although **2** could be easily isolated, the formyl group of **2** was reduced to yield

corresponding alcohols **5** for the determination of the stereochemical outcome, as shown in Table 1. Branched and

Table 1. Substrate Scope of Sequential Transformation of 4 into β -Amino Aldehydes 2 via 1 Followed by Reduction of Formyl Group^a

entry	4 (R)	1 (Z)/ (E)	conditions ^b	5	yield (%) ^c (<i>anti</i> / <i>syn</i>)	ee (%) ^d
1	4a: Bn	98:2 ^e	acetone, 40 °C, 7 h	5a	70 (95:5)	94
2	4b: Me	97:3 ^f	AcOEt, 40 °C, 2 h	5b	86 (91:9)	76
3	4c: <i>n</i> -pentyl	96:4 ^f	acetone, 40 °C, 7 h	5c	76 (93:7)	97
4	4d: <i>i</i> -butyl	96:4 ^f	AcOEt, 40 °C, 3 h	5d	55 (95:5)	97
5	4e: <i>c</i> -hexyl	95:5 ^f	AcOEt, 40 °C, 3 h	5e	75 (95:5)	>99
6	4f: Ph	96:4 ^f	AcOEt, 40 °C, 3 h	5f	87 (93:7)	98

^aAll reactions were carried out using 0.25 mmol of allyl hemiaminal ether **4**. ^bReaction conditions for enantioselective APF rearrangement. ^cCombined yield of *anti*/*syn*-**5** from **4** (three steps). ^dFor major *anti*-**5**. Determined by chiral stationary phase HPLC analysis. Absolute stereochemistry of *anti*-**5a** was determined to be 2*R*,3*R*-configuration. See Supporting Information for details. ^eIsomerization of allyl hemiaminal ether **4** using NiI₂(*p*-tolbiphep). ^fIsomerization of allyl hemiaminal ether **4** using NiI₂(dppf).

linear aliphatic substituents were well tolerated and the sequential transformation enabled to afford corresponding γ -amino- γ -alkyl alcohols **5** in high *anti*- and enantioselectivities (up to 95% *anti*, >99% ee) (entries 1, 3–5), with the exception of the less sterically hindered methyl substituent (entry 2). Remarkably, the optimized sequential protocol that was originally developed for aliphatic substrates was also applicable to aromatic hemiaminal ethers, giving rise to γ -amino- γ -aryl alcohol **5f** with high *anti*- and enantioselectivities (entry 6).

In spite of those intriguing findings, however, some issues related to the stereoselective APF rearrangement catalyzed by chiral phosphoric acid remain, including

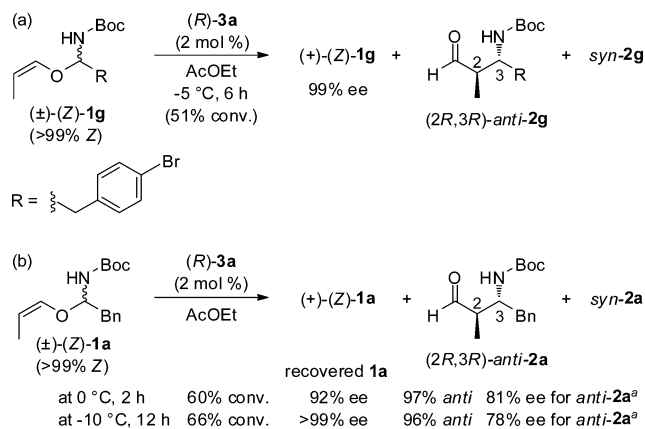
- Determination of the absolute configuration of recovered hemiaminal vinyl ether **1** under the influence of chiral phosphoric acid catalyst (*R*)-**3** to elucidate the mechanisms of the optical kinetic resolution of racemic hemiaminal vinyl ether **1**.
- Mechanistic investigations of the optical kinetic resolution of racemic hemiaminal vinyl ether **1** by chiral phosphoric acid (*R*)-**3**, where experiments using enantiomerically pure hemiaminal vinyl ether **1** would be helpful to validate the stereochemical relationship between hemiaminal vinyl ethers **1** and β -amino- β -alkyl aldehydes **2**.
- Detailed experimental studies to justify the anomalous temperature effect, that is, the increase in enantioselectivity with increasing reaction temperature.
- Theoretical studies on the transition states to rationalize the stereochemical outcome of entire process consisting of the C–O bond cleavage and the C–C bond formation steps.

- (e) Comprehensive mechanistic considerations to understand the enantioconvergent process in which racemic hemiaminal vinyl ether **1** was efficiently transformed into optically active β -amino- β -alkyl aldehydes **2** under the influence of chiral phosphoric acid catalyst (*R*)-**3**.

In order to address those issues, we focused our efforts on the elucidation of the overall scheme of the stereochemical relationship in the present fascinating rearrangement by conducting detailed and extensive studies on the mechanisms of *anti*- and enantioselective APF rearrangement, including (A) X-ray crystallographic analysis of the recovered hemiaminal vinyl ether to determine the absolute stereochemistry, (B) experiments of enantiomerically pure hemiaminal vinyl ethers to understand the stereochemical outcome, (C) transition state analysis by computational studies, and (D) crossover experiments of two hemiaminal vinyl ethers having different vinyl ether and aliphatic (*R*) substituents.

Experiment A: Determination of the Absolute Configuration of Recovered Hemiaminal Ether. As shown in Scheme 1, of particular interest is the efficient optical kinetic resolution of racemic hemiaminal ether (*Z*)-**1a** at the C–O bond cleavage step. At the outset of mechanistic studies of the APF rearrangement, we began by determining the absolute configuration of recovered hemiaminal vinyl ether (*Z*)-**1a**. In order to determine the absolute stereochemistry of the hemiaminal vinyl ether by X-ray crystallographic analysis, we employed structurally similar hemiaminal vinyl ether (*Z*)-**1g** that has a bromo substituent at the *para*-position of the phenyl ring. To obtain enantiomerically pure (*Z*)-**1g**, we performed the optical kinetic resolution of racemic (*Z*)-**1g** using 2 mol % of phosphoric acid (*R*)-**3a** instead of (*R*)-**3b** (Scheme 2a) because

Scheme 2. Optical Kinetic Resolution of Hemiaminal Vinyl Ethers (*Z*)-**1a** and (*Z*)-**1g** Using Catalyst (*R*)-**3a**



^aThe % ee of **2a** was determined after reduction of formyl group to alcohol.

of the availability of catalyst **3a**. As shown in Scheme 2b, efficient optical kinetic resolution of (*Z*)-**1a** was also achieved by using phosphoric acid (*R*)-**3a** as the resolving catalyst, although lowering of the reaction temperature was required to obtain enantiomerically pure (*Z*)-**1a** in good yield. The optical kinetic resolution of racemic (*Z*)-**1g** was conducted at -5 °C for 6 h. (*Z*)-**1g** was converted into **2g** in 51% yield and recovered in 28% isolated yield (48% NMR yield) in a nearly enantiomerically pure form (99% ee) after preparative HPLC purification.

Thus, recovered optically active hemiaminal vinyl ether (+)-(*Z*)-**1g** (99% ee) was recrystallized from ether under pentane vapor to give an X-ray grade single crystal. X-ray crystallographic analysis of recovered **1g** indicated that the absolute stereochemistry of (+)-**1g** was the (*S*)-configuration (Figure 4).²³ The confirmed stereochemical outcome using (*Z*)-**1g** should be applicable to that observed in the optical kinetic resolution of racemic (*Z*)-**1a** (Scheme 1). Under the influence of (*R*)-**3b**, (*R*)-(-)-(*Z*)-**1a** reacted much more rapidly than (*S*)-(+)-(*Z*)-**1a** that was recovered in an enantiomerically pure form.

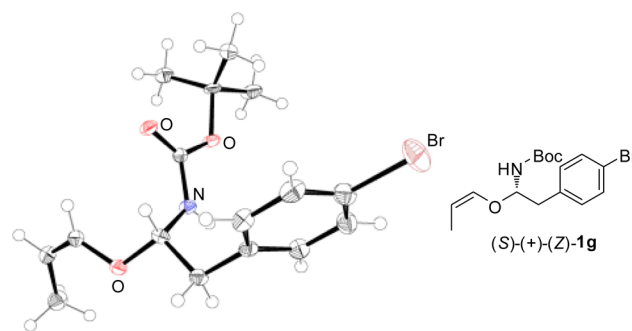
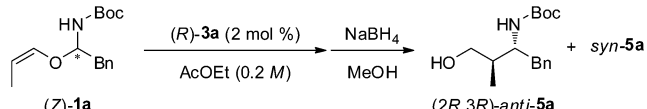
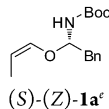
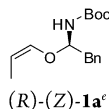
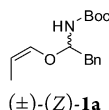
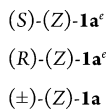
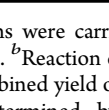
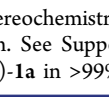


Figure 4. ORTEP drawing of (*S*)-(+)-(*Z*)-**1g** with probability ellipsoids drawn at the 50% level.

Experiment B: Aza-Petasis–Ferrier Rearrangement of Enantiomerically Pure Hemiaminal Ethers.

In order to gain a precise understanding of the stereochemical relationship between starting (*Z*)-**1a** and rearranged product **2a**, we performed the APF rearrangement using both enantiomers of (*Z*)-**1a** in an enantiomerically pure form. The enantiomers of (*Z*)-**1a** were separated by chiral stationary phase HPLC to afford each enantiomer in a pure form. Thus, prepared (*S*)-(*Z*)-**1a** and (*R*)-(*Z*)-**1a** were subjected to the APF rearrangement individually in the presence of (*R*)-**3a**. The rearrangement was performed at 40 and 0 °C in ethyl acetate using 2 mol % of (*R*)-**3a** and was followed by the reduction of **2a** to give rise to corresponding alcohol (2*R*,3*R*)-*anti*-**5a** as the major stereoisomer in good yields in all cases (Table 2). The results obtained by using the racemic mixture of (*Z*)-**1a** are also displayed for reference (entries 3 and 6). As expected from the efficient optical kinetic resolution observed in the present rearrangement (Schemes 1 and 2), the reaction of (*R*)-(*Z*)-**1a** proceeded much more rapidly than that of (*S*)-(*Z*)-**1a** at both 40 and 0 °C (entries 2 vs 1 and 5 vs 4). Although (*S*)-(*Z*)-**1a** underwent the rearrangement sluggishly, the enantioselectivities were the highest compared with those observed for the opposite enantiomer (*R*)-(*Z*)-**1a** and racemic (\pm)-(*Z*)-**1a** (entry 1 vs 2 and 3 and entry 4 vs 5 and 6). More importantly, in the reaction of (*S*)-(*Z*)-**1a**, the enantioselectivities increased with decreasing reaction temperature as observed in typical catalytic enantioselective reactions (entry 1 vs 4). Indeed, nearly enantiomerically pure **5a** was afforded at 0 °C (entry 4). In sharp contrast, the reaction of (*R*)-(*Z*)-**1a** resulted in a considerable decrease in enantioselectivity when the reaction temperature was lowered from 40 to 0 °C (entry 2 vs 5). This anomalous temperature effect was detected in our preliminary studies on the APF rearrangement of (\pm)-(*Z*)-**1a** (entry 3 vs 6).⁸ It can be readily expected that the enantioselectivity observed in the reaction of (\pm)-(*Z*)-**1a** is the intermediate of those observed in the reaction of (*S*)-(*Z*)-**1a** and (*R*)-(*Z*)-**1a**

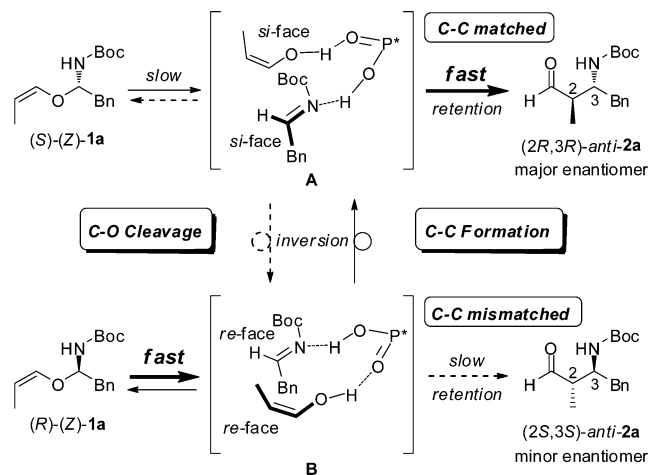
Table 2. APF Rearrangement of Enantiomerically Pure and Racemic (Z)-1a Catalyzed by (R)-3a^a


entry	1a	conditions ^b	yield (%) ^c	<i>anti</i> - 5a / <i>syn</i> - 5a	ee (%) ^d
1		40 °C, 2 h	84	98 : 2	95
2		40 °C, 10 min	95	98 : 2	90
3		40 °C, 1.5 h	92	97 : 3	92
4		0 °C, 36 h	78	99 : 1	99
5		0 °C, 4 h	81	97 : 3	77
6		0 °C, 30 h	75	97 : 3	87

^aAll reactions were carried out using 0.1 mmol of hemiaminal vinyl ether (**Z**)-**1a**. ^bReaction conditions for enantioselective APF rearrangement. ^cCombined yield of *anti*/*syn*-**5a** from **1a** (two steps). ^dFor major *anti*-**5a**. Determined by chiral stationary phase HPLC analysis. Absolute stereochemistry of *anti*-**5a** was determined to be 2*R*,3*R*-configuration. See Supporting Information for details. ^eEnantiomeric purity of (**Z**)-**1a** in >99% ee.

(entries 3 vs 1 and 2, and 6 vs 4 and 5) because (±)-(**Z**)-**1a** is a mixture of equal amounts of (*S*)- and (*R*)-(**Z**)-**1a**.

The stereochemical relationship between starting (**Z**)-**1a** and corresponding product **5a** (derived from **2a**) should be noted in the present APF rearrangement. The stereogenic center of starting (**Z**)-**1a** is lost during the course of the rearrangement. The newly generated stereogenic center of product **5a** has (2*R*,3*R*)-configuration in all cases, despite the fact that the absolute configuration of enantiomeric (**Z**)-**1a** is the opposite. The reaction of (*S*)-(**Z**)-**1a** proceeded with retention at the stereogenic center bearing an *N*-Boc amino group, whereas (*R*)-(**Z**)-**1a** exhibited inversion at that stereogenic center. From experimental evidence obtained using enantiomerically pure substrates (**Z**)-**1a** (Table 2), a plausible mechanism of the present rearrangement is proposed, as illustrated in Figure 5. Under the influence of (*R*)-**3**, (*S*)-(**Z**)-**1a** undergoes C–O cleavage sluggishly to generate intermediate **A**. However, the subsequent C–C bond formation of intermediate **A** is favored in the presence of (*R*)-**3**, because the highest enantioselectivity was observed in the reaction of (*S*)-(**Z**)-**1a**. It can be considered that the combination of (*R*)-**3** and intermediate **A** generated from (*S*)-(**Z**)-**1a** is a matched pair of their chiralities for C–C bond formation (C–C matched). More importantly, during the course of the rearrangement, C–O bond cleavage and C–C bond formation proceed on the same side of the enantiotopic face, that is, the *si* face, of the imine fragment in intermediate **A**. Consequently, the retention process dominates the overall scheme of the present rearrangement despite the slow C–O bond cleavage. In contrast, (*R*)-(**Z**)-**1a** undergoes C–O bond

**Figure 5.** Plausible mechanism of APF rearrangement catalyzed by chiral phosphoric acid (*R*)-**3**.

cleavage rapidly to generate intermediate **B**. However, the subsequent C–C bond formation of intermediate **B** via a retentive manner is retarded by (*R*)-**3**. Accordingly, the chiral information on (*R*)-(**Z**)-**1a** is unfavorable for the C–C bond formation under the influence of (*R*)-**3** (C–C mismatched), and hence, the rearrangement would proceed via an inversion process. The low enantioselectivities of product *anti*-**5a** obtained from (*R*)-(**Z**)-**1a** imply that the unfavorable retentive process from intermediate **B** partially participates in the rearrangement. The anomalous temperature effect observed in the reactions of (*R*)-(**Z**)-**1a** and (±)-(**Z**)-**1a** may be due to the loss of unfavorable chiral information at higher temperature because the enantioselectivities increase in those cases.

Experiment C: Computational Studies of Transition States. The significant differences in the reaction rates between enantiomers (**Z**)-**1a** and the intriguing stereochemical relationship between starting (**Z**)-**1a** and rearranged product **2a** prompted us to further study the mechanism of the catalytic enantioselective APF rearrangement in detail. In the previous section, we proposed a plausible mechanism of the present rearrangement. However, (i) the efficient optical kinetic resolution, (ii) the predominant formation of the *anti*-isomer having the (2*R*,3*R*)-configuration from the (**Z**)-substrate, and (iii) the overall scheme of the present enantioconvergent process remain to be elucidated. Therefore, we theoretically studied the mechanism of the present APF rearrangement in combination with the above experimental observations. Catalyst (*R*)-**3b** and substrate (**Z**)-**1a** were used for the theoretical studies.

All calculations were performed with the Gaussian 09 program.²⁴ Geometries were fully optimized and characterized by frequency calculation using the ONIOM method,²⁵ combining the B3LYP (Becke's three-parameter hybrid method^{26a} using the Lee–Yang–Parr correlation functional^{26b}) density functional theory (DFT) with the 6-31G(d) basis set²⁷ in the low-level layer and the Møller–Plesset perturbation theory second-order correction (MP2)²⁸ with the 6-31+G(d,p) basis set²⁹ in the high-level layer. The atom distribution in those two layers is shown in Figure 8, where atoms in the high level layer are represented by a “ball & bond type” model and atoms in the low level layer by a “tube” model. Free energies (298.15 K, 1 atm) were initially computed for the gas phase. The geometrically optimized structures were further calculated

for the continuum solvation model, where the single-point energy calculation with the self-consistent reaction field (SCRF) method based on the polarizable continuum model (CPCM,³⁰ $\epsilon = 5.9867$ for ethyl acetate) was carried out at the same level as the one used for geometry optimization. The free energies in ethyl acetate were calculated from the sum of the single-point energies in ethyl acetate and the value of thermal correction to Gibbs free energy in gas phase.

As postulated in Figure 5, it seems that the rearrangement is composed of two transformation steps: C–O bond cleavage and C–C bond formation. Therefore, we calculated the transition states of those two steps individually. The calculation was started at the C–O bond cleavage step, where the first issue of efficient optical kinetic resolution is the main subject to be addressed. On the basis of the acid/base dual function of phosphoric acid catalyst **3**,^{21f,g,31} it can be considered that the C–O bond cleavage is mediated by the protonation of the ether oxygen atom of hemiaminal vinyl ether (*Z*)-**1a** by the Brønsted acidic proton of (*R*)-**3b**, whereas the Lewis basic phosphoryl oxygen interacts with the N–H proton of the hemiaminal, forming two parallel hydrogen bonds between (*Z*)-**1a** and (*R*)-**3b**, as illustrated in Figure 6. Eight initial TS structures are generated from the two absolute configurations of (*Z*)-**1a** (*R* and *S*; $\text{TS}_{\text{co}r}$ and $\text{TS}_{\text{co}s}$), the two protonation sites at the ether oxygen atom of (*Z*)-**1a**, and the two orientations of the vinyl ether moiety.³²

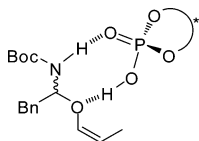


Figure 6. Two-point binding model for the C–O bond cleavage step through the formation of parallel hydrogen bonds between (*Z*)-**1a** and (*R*)-**3b**.

Among the possible transition structures searched under the influence of (*R*)-**3b**, the energetically favorable transition structures of $\text{TS}_{\text{co}r}$ for (*R*)-(*Z*)-**1a** and $\text{TS}_{\text{co}s}$ for (*S*)-(*Z*)-**1a** are shown in Figure 7.³³ $\text{TS}_{\text{co}r1}$ is the most favorable transition state as it is 2.9 kcal/mol lower in energy than $\text{TS}_{\text{co}s1}$. This result is consistent with the experimental result that the optical kinetic resolution of racemic (*Z*)-**1a** gave rise to enantiomerically pure (*S*)-(*Z*)-**1a** as the recovery of the starting substrate

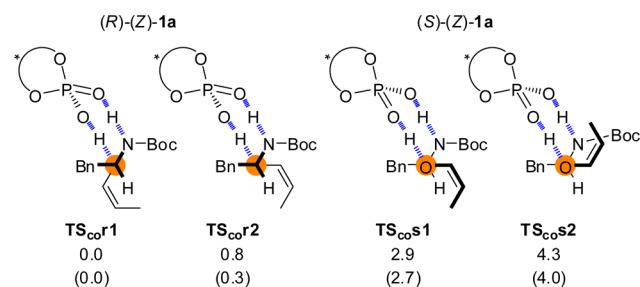


Figure 7. Schematic representation models of energetically favorable $\text{TS}_{\text{co}r}$ and $\text{TS}_{\text{co}s}$. Relative free energies (kcal/mol) obtained by single-point energy calculations with the SCRF method based on CPCM ($\epsilon = 5.9867$ for ethyl acetate) are shown. Relative free energies (kcal/mol) of the optimized structures in the gas phase are shown in parentheses.

even with approximately 50% conversion of (*Z*)-**1a** (Scheme 1).

Structural analysis of the most energetically favorable transition states for each substrate, $\text{TS}_{\text{co}r1}$ and $\text{TS}_{\text{co}s1}$ (Figure 8), allowed us to identify the major factors contributing to the efficient optical kinetic resolution. In the most favorable $\text{TS}_{\text{co}r1}$ (Figure 8a), the imine fragment of substrate (*R*)-(*Z*)-**1a** is almost parallel to the aryl plane of the catalyst substituent (G: 4-*tert*-butyl-2,6-diisopropylphenyl) to avoid steric congestion. In contrast, the imine fragment of substrate (*S*)-(*Z*)-**1a** in $\text{TS}_{\text{co}s1}$ is oriented perpendicularly to the aryl plane of the catalyst substituent (G) (Figure 8b), where both the *N*-Boc group and the benzyl moiety of substrate (*S*)-(*Z*)-**1a** are located close to the aryl substituent (G). This leads to steric repulsion between the substrate and the catalyst (indicated by red curved double-headed arrows), which would be responsible for the destabilization of $\text{TS}_{\text{co}s1}$.

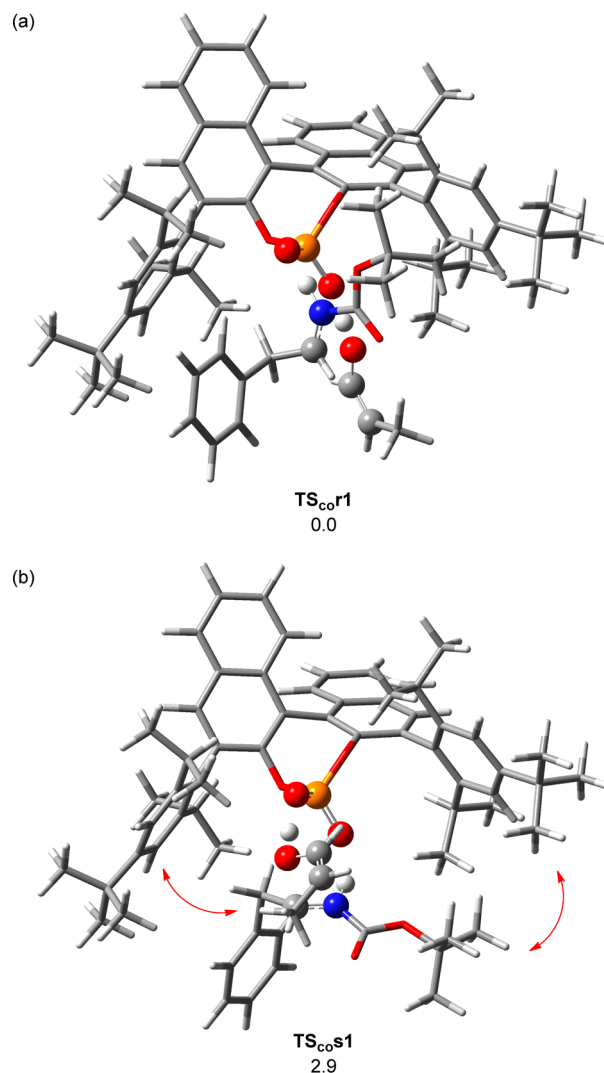


Figure 8. 3D structures of the most energetically favorable transition states for the C–O bond cleavage step are shown (the high level layer and the low level layer are represented by “ball & bond type” and “tube” models, respectively): (a) (*R*)-(*Z*)-**1a** for $\text{TS}_{\text{co}r1}$. (b) (*S*)-(*Z*)-**1a** for $\text{TS}_{\text{co}s1}$. Relative free energies (kcal/mol) in the solution phase are also shown.

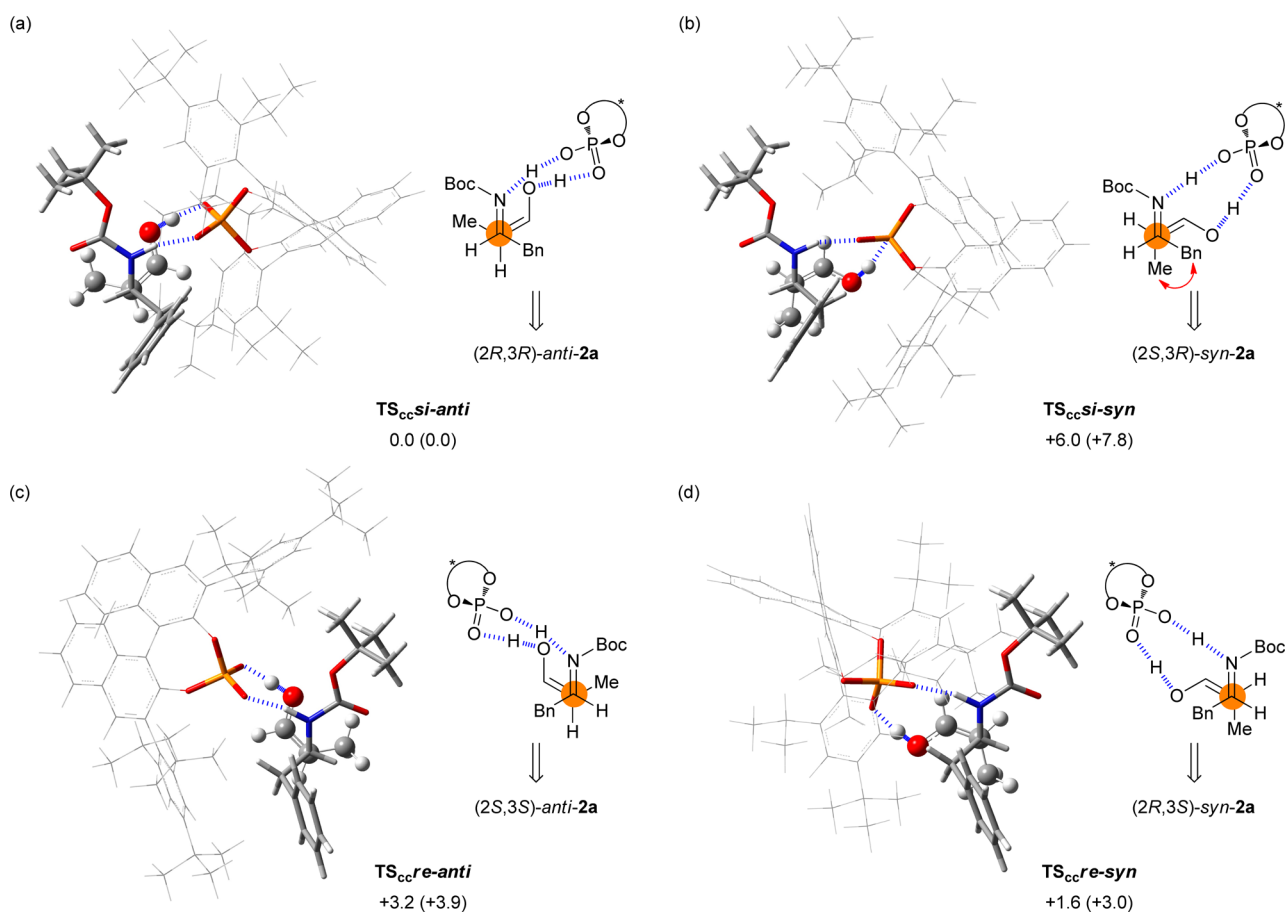


Figure 9. 3D structures and schematic representation models of four transition states for the C–C bond formation step. The 3D structures of each fragment are represented as follows: imine fragment and phosphoric acid subunit, “tube” model; enol fragment, “ball & bond type” model; and binaphthyl backbone and substituent (G), “wire” model. Relative free energies (kcal/mol) obtained by single-point energy calculations with the SCRF method based on CPCM ($\epsilon = 5.9867$ for ethyl acetate) are shown. In parentheses are the relative free energies (kcal/mol) of the optimized structures in the gas phase. (a) $\text{TS}_{\text{ccsi-anti}}$: Bond formation between *si* face of imine and *si* face of enol to give (2*R*,3*R*)-*anti*-2a. (b) $\text{TS}_{\text{ccsi-syn}}$: Bond formation between *si* face of imine and *re* face of enol to give (2*S*,3*R*)-*syn*-2a. (c) $\text{TS}_{\text{ccre-anti}}$: Bond formation between *re* face of imine and *re* face of enol to give (2*S*,3*S*)-*anti*-2a. (d) $\text{TS}_{\text{ccre-syn}}$: Bond formation between *re* face of imine and *si* face of enol to give (2*R*,3*S*)-*syn*-2a.

Further calculations were carried out to acquire a mechanistic insight into the C–C bond formation step, where the second issue of the predominant formation of the (2*R*,3*R*)-*anti*-isomer is the main subject to be addressed. On the basis of the acid/base dual function of phosphoric acid catalyst **3**,³¹ the imine and the enol, generated in situ via the C–O bond cleavage, interact with chiral phosphoric acid (*R*)-**3b** through two hydrogen bonds, as illustrated in Figure 5. As shown in Figure 9, a thorough search of the transition structures afforded four possible stereoisomers of **2a** and resulted in the successful optimization of the four transition states. Among the four diastereomeric transition states displayed, the most energetically favorable transition state is $\text{TS}_{\text{ccsi-anti}}$, which affords (2*R*,3*R*)-*anti*-2a (Figure 9a). The formation of the (2*R*,3*R*)-isomer is consistent with the experimental result that the rearrangement under the influence of (*R*)-**3** resulted in the production of (2*R*,3*R*)-*anti*-2a as the major stereoisomer, irrespective of the chirality of starting (*Z*)-**1a** (see Table 2). The preferential formation of (2*R*,3*R*)-*anti*-2a over the *syn*-isomer is well rationalized by the structural analysis of the transition states. In particular, when the *si* face of the imine reacts with enol, $\text{TS}_{\text{ccsi-anti}}$ (Figure 9a) is 6.0 kcal/mol lower in energy than $\text{TS}_{\text{ccsi-syn}}$ (Figure 9b), despite the structural resemblance of those two transition states with the exception of

the enol orientation.³⁴ The relative positions of the methyl substituent of the enol and the benzyl substituent of the imine are responsible for the marked energy difference between $\text{TS}_{\text{ccsi-anti}}$ and $\text{TS}_{\text{ccsi-syn}}$ (indicated by a red curved double-headed arrow). Indeed, the methyl and benzyl groups assume an *anti*-conformation in $\text{TS}_{\text{ccsi-anti}}$, whereas the gauche interaction between the methyl and benzyl groups results in the destabilization of $\text{TS}_{\text{ccsi-syn}}$.

Detailed structural analysis of $\text{TS}_{\text{ccsi-anti}}$ and $\text{TS}_{\text{ccre-anti}}$ allowed us to identify the origin of the high enantioselectivity (Figure 10). As shown in Figure 10a, in $\text{TS}_{\text{ccsi-anti}}$, the imine fragment is positioned vertically and shows no detrimental repulsive interaction with the catalyst substituent (G), affording (2*R*,3*R*)-*anti*-2a predominantly. In contrast, the imine fragment in $\text{TS}_{\text{ccre-anti}}$ is horizontally oriented (Figure 10b), leading to repulsive interactions between the catalyst substituent (G) and both the *N*-Boc and benzyl groups of the imine fragment (indicated by red curved double-headed arrows), and thereby destabilizing $\text{TS}_{\text{ccre-anti}}$ and preventing the formation of (2*S*,3*S*)-*anti*-2a.

Using the energy profiles of the C–O bond cleavage and C–C bond formation steps in the present APF rearrangement summarized in Figure 11, the third issue of the clarification of the enantioconvergent process is addressed. It is worthy of note

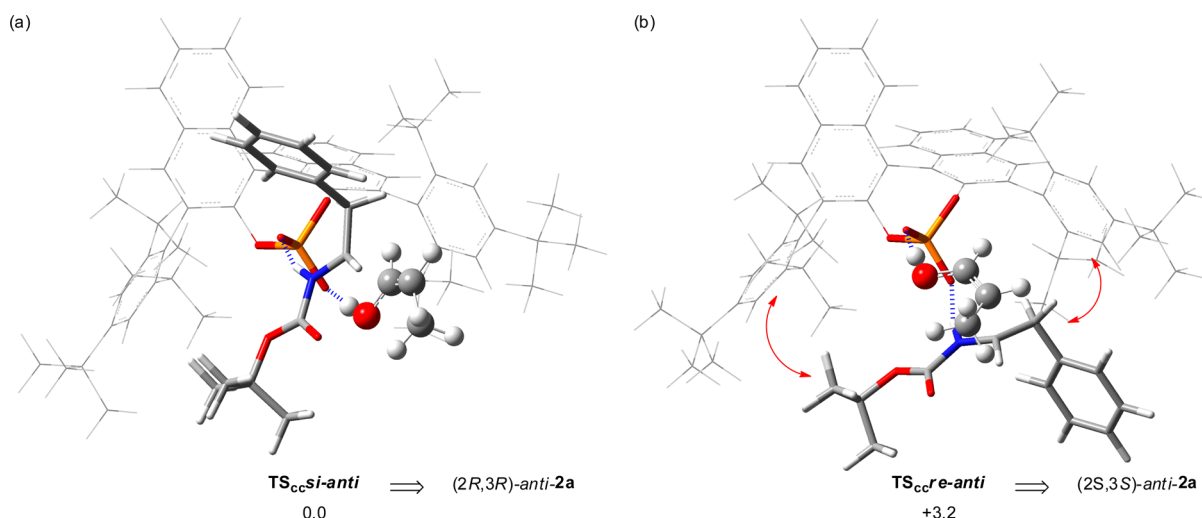


Figure 10. 3D structures of transition states for C–C bond formation step giving *anti*-2a. (a) $\text{TS}_{\text{cc}}^{\text{si-anti}}$: *si* face/*si* face giving $(2R,3R)\text{-anti-2a}$. (b) $\text{TS}_{\text{cc}}^{\text{re-anti}}$: *re* face/*re* face giving $(2S,3S)\text{-anti-2a}$. The 3D structures are represented in accordance with Figure 9. Relative free energies (kcal/mol) in the solution phase are also shown.

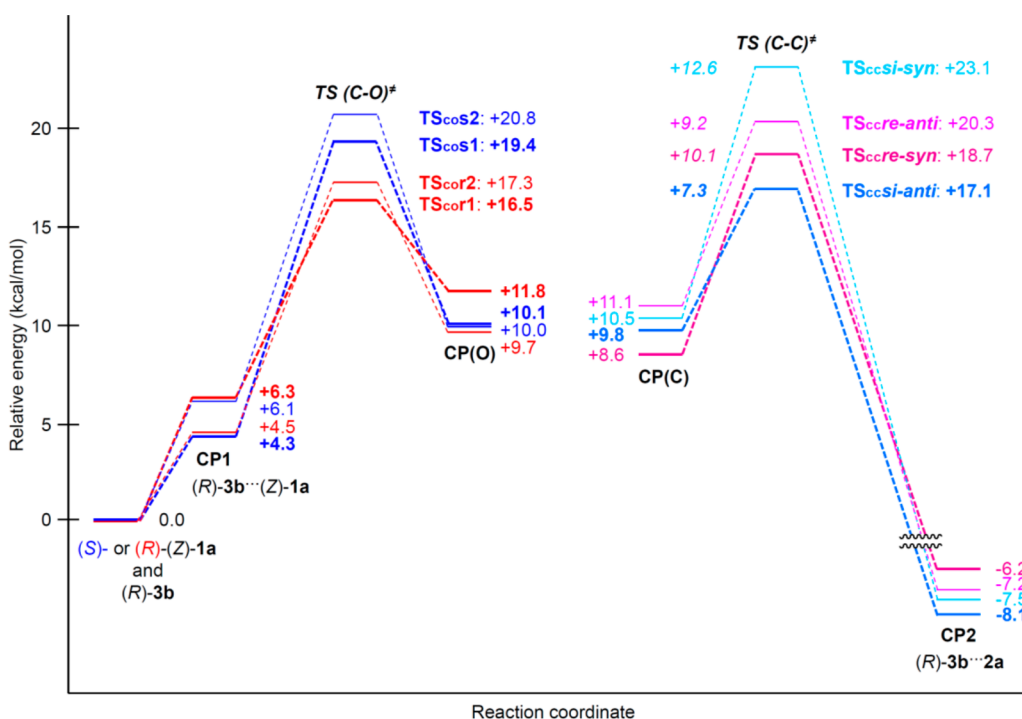


Figure 11. Energy profiles of C–O bond cleavage and C–C bond formation steps. The relative free energy (kcal/mol) of the sum of $(Z)\text{-1a}$ and $(R)\text{-3b}$ is set to zero. The results of single-point energy calculations with the SCRf method based on CPCM ($\epsilon = 5.9867$ for ethyl acetate) are shown. Activation energies are shown in italic.

that the proposed reaction mechanism depicted in Figure 5 can be rationalized by the present energy profile without acute contradiction. $(S)\text{-}(Z)\text{-1a}$ undergoes C–O bond cleavage through the higher energy transition state TS_{ccor1} under the influence of $(R)\text{-3b}$. In fact, the C–O bond cleavage of $(S)\text{-}(Z)\text{-1a}$ proceeds sluggishly compared with that of $(R)\text{-}(Z)\text{-1a}$, even if efficient optical kinetic resolution is achieved. However, in the subsequent C–C bond formation step, the *si* face of the imine fragment reacts with enol via the energetically lowest transition state $\text{TS}_{\text{cc}}^{\text{si-anti}}$ under the influence of $(R)\text{-3b}$, giving rise to $(2R,3R)\text{-anti-2a}$ exclusively. The *si* face of the imine fragment generated from $(S)\text{-}(Z)\text{-1a}$ is the same enantiotopic face where

the C–O bond cleavage takes place. Consequently, $(S)\text{-}(Z)\text{-1a}$ undergoes the rearrangement in a retentive manner at the stereogenic center bearing the *N*-Boc amino group, where the initial chiral information on $(S)\text{-}(Z)\text{-1a}$ is favorable for the subsequent C–C bond formation (C–C matched), albeit the sluggish rearrangement. In contrast, the C–O bond cleavage of $(R)\text{-}(Z)\text{-1a}$ proceeds more rapidly than that of $(S)\text{-}(Z)\text{-1a}$ because of the energetically lower transition state of TS_{ccor1} (or TS_{ccor2}) for $(R)\text{-}(Z)\text{-1a}$ under the influence of $(R)\text{-3b}$. However, the subsequent C–C bond formation at the *re* face of imine ($\text{TS}_{\text{cc}}^{\text{re-syn}}$ or $\text{TS}_{\text{cc}}^{\text{re-anti}}$), which originates from the same enantiotopic face as that of the C–O bond cleavage of the

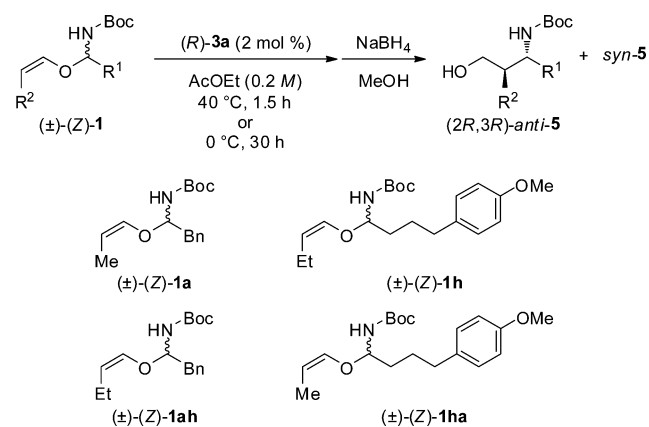
(*R*)-substrate, is energetically unfavorable (C–C mismatched). Hence, the C–C bond formation proceeds through the energetically lowest transition state TS_{cc} -*anti*, affording (2*R*,3*R*)-*anti*-**2a** as the major stereoisomer, where the inversion at the stereogenic center bearing the *N*-Boc amino group is enhanced by (*R*)-**3b** at the C–C bond formation step. As mentioned above, the intriguing enantioconvergent process observed in this rearrangement can be rationalized on the basis of the present energy profiles. In addition, it seems that the present two-step sequential transformation is rate-determined by C–O bond cleavage of both enantiomers of (*Z*)-**1a**. However, the mode of reaction is dependent on the chirality of substrate (*Z*)-**1a**. In the rearrangement of (*S*)-(*Z*)-**1a**, it is reasonable to suggest that C–O bond cleavage is effectively irreversible because C–C bond formation is lower in energy than the backward pathway of C–O bond formation. On the other hand, in the rearrangement of (*R*)-(*Z*)-**1a**, the equilibrium of C–O bond cleavage and formation between (*R*)-(*Z*)-**1a** and intermediate **B** would likely proceed during the whole reaction process (Figure 5).

Experiment D: Crossover Experiments of Two Hemiaminal Vinyl Ethers. The theoretical studies strongly support our mechanistic proposal for the present intriguing rearrangement. However, whether the inversion observed in the rearrangement of (*R*)-(*Z*)-**1a** proceeds in an *intramolecular* manner is still unclear. To enhance our understanding of the inversion process and to determine the overall scheme of the present enantioconvergent process, we conducted crossover experiments of (*Z*)-**1a** and (*Z*)-**1h**. Before starting the crossover experiments, we collected reference data of the APF rearrangement of (\pm)-(*Z*)-**1a**, (\pm)-(*Z*)-**1h**, (\pm)-(*Z*)-**1ah**, and (\pm)-(*Z*)-**1ha**. The rearrangement of racemic substrates (*Z*)-**1** was performed using 2 mol % of (*R*)-**3a** at 40 °C for 1.5 h and at 0 °C for 30 h in ethyl acetate, followed by the reduction of corresponding products **2** with sodium borohydride to determine the stereoselectivities of the products. The stereochemical outcomes of those reference reactions are summarized in Table 3.

As shown in Table 3, all substrates (*Z*)-**1** exhibited a similar reactivity to afford corresponding products **5** in good to excellent yields with high *anti*-selectivities. The anomalous temperature effect was also observed in all of the substrates, that is, the enantioselectivities increased as the reaction temperature increased. In addition, hemiaminal vinyl ethers having a (4-methoxyphenyl)propyl group at the stereogenic center, (\pm)-(*Z*)-**1h** and (\pm)-(*Z*)-**1ha** (entries 3, 4, 7, and 8), exhibited higher enantioselectivities than the benzyl-substituted ones, (\pm)-(*Z*)-**1a** and (\pm)-(*Z*)-**1ah** (entries 1, 2, 5, and 6). In contrast, the substituent at the terminal of the vinyl ether moiety had no influence on the enantioselectivity (entries 1 vs 5, 2 vs 6, 3 vs 7, and 4 vs 8) and nearly equal enantioselectivities were obtained by changing the substituent from methyl to ethyl [(*Z*)-**1a** \rightarrow (*Z*)-**1ah**, (*Z*)-**1ha** \rightarrow (*Z*)-**1h**] under each set of reaction conditions.

In principle, in the crossover experiment between (*Z*)-**1a** and (*Z*)-**1h**, **5a** and **5h** should be the exclusive products via the *intramolecular* pathway. In contrast, the *intermolecular* exchange process would afford not only cross-products **5ah** and **5ha** but also normal-products **5a** and **5h**, as shown in Figure 12. The estimated participation of the normal *intermolecular* process during the whole transformation can be statistically calculated to be twice that of the cross-products. For instance, the cross- and normal-products would be

Table 3. APF Rearrangement of Racemic (*Z*)-**1** Catalyzed by (*R*)-**3a** as Reference for Crossover Experiments^a



entry	1	conditions ^b	5	yield (%) ^c	<i>anti</i> -5/ <i>syn</i> -5	ee (%) ^d
1	(\pm)-(<i>Z</i>)- 1a	40 °C, 1.5 h	5a	92	97:3	92
2		0 °C, 30 h		75	97:3	87
3	(\pm)-(<i>Z</i>)- 1h	40 °C, 1.5 h	5h	94	95:5	98
4		0 °C, 30 h		92	93:7	96
5	(\pm)-(<i>Z</i>)- 1ah	40 °C, 1.5 h	5ah	88	97:3	92
6		0 °C, 30 h		74	96:4	86
7	(\pm)-(<i>Z</i>)- 1ha	40 °C, 1.5 h	5ha	90	97:3	98
8		0 °C, 30 h		95	96:4	97

^aAll reactions were carried out using 0.1 mmol of hemiaminal vinyl ether (*Z*)-**1**. ^bReaction conditions for enantioselective APF rearrangement. ^cCombined yield of *anti*/*syn*-**5** from **1** (two steps). ^dFor major *anti*-**5**. Determined by chiral stationary phase HPLC analysis.

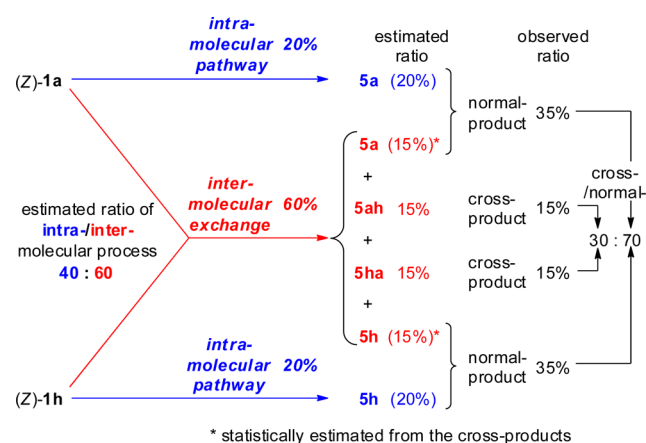
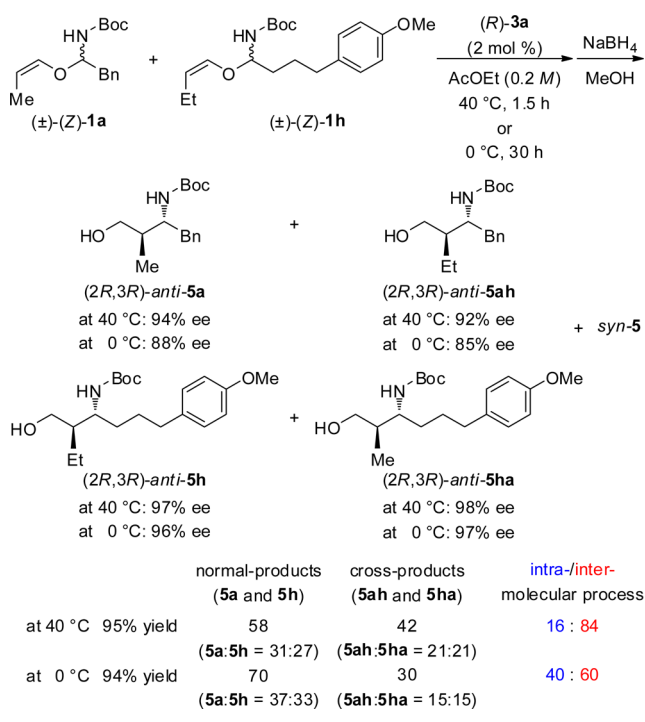


Figure 12. Projected product distributions from the crossover experiments.

obtained in a ratio of 30 (**5ah**:**5ha** = 15:15) to 70 (**5a**:**5h** = 35:35), respectively, in which the percentage of the *intermolecular* exchange process is estimated to be 60%, that is, twice the 30% proportion of the cross-products. In addition, to simplify our analysis of the crossover experiments, we focused on the isomeric ratios of major *anti*-**5** because less than 5% *syn*-**5** is formed in most cases, as based on the reference data.

Bearing the above considerations in mind, we began by performing the crossover experiments of racemic substrates (\pm)-(*Z*)-**1a** and (\pm)-(*Z*)-**1h** under the same conditions as those for the reference reaction using an equimolar mixture of substrates (\pm)-(*Z*)-**1**. As shown in Scheme 3, considerable

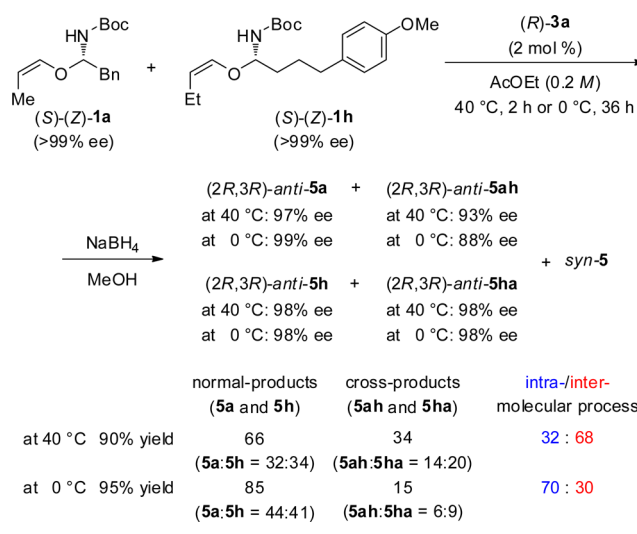
Scheme 3. Crossover Experiments of Racemic (Z)-1a and (Z)-1h



amounts of cross-products **5ah** and **5ha** were obtained (at 40 °C, 42%; at 0 °C, 30%), although normal-products **5a** and **5h** were formed mainly.³⁵ The results strongly suggest that the rearrangement proceeds predominantly through an *intermolecular* exchange process because normal-products **5a** and **5h** are also formed in the intermolecular process, as shown in Figure 12. Here, the percentage of the intermolecular exchange process can be estimated to be 84% (42 × 2) and 60% (30 × 2) at 40 and 0 °C, respectively, on the basis of the above considerations. By taking into account of estimated proportion of intra/intermolecular processes (16:84) at high reaction temperature, it is interesting to note that most of the rearrangements took place via an intermolecular exchange process. As expected, the enantioselectivities observed in both normal- and cross-products **5** are nearly identical with those obtained from individual reference reactions within experimental error (Scheme 3 vs Table 3).

Further crossover experiments were conducted using enantiomerically pure substrates to gain an insight into the intermolecular exchange process as observed in the reaction of the racemic substrates. The C–C matched combination of (S)-(Z)-1 and (R)-3a was investigated first. Crossover experiments of (S)-(Z)-1a and (S)-(Z)-1h were performed under the same reaction conditions as those for the crossover experiments of the racemic substrates. As shown in Scheme 4, the ratios of cross-products **5ah** and **5ha** were markedly reduced in comparison with those observed in the reaction of the racemic substrates (Scheme 4 vs Scheme 3).³⁶ At the low temperature (0 °C), the participation of the intermolecular exchange process was significantly suppressed and the intramolecular pathway predominated in the C–C matched combination (the estimated percentages of the intramolecular pathway are 70% at 0 °C and 32% at 40 °C). As expected, higher enantioselectivities were observed for normal-products **5a** and **5h** than for those obtained in the crossover experiments of racemic (Z)-1

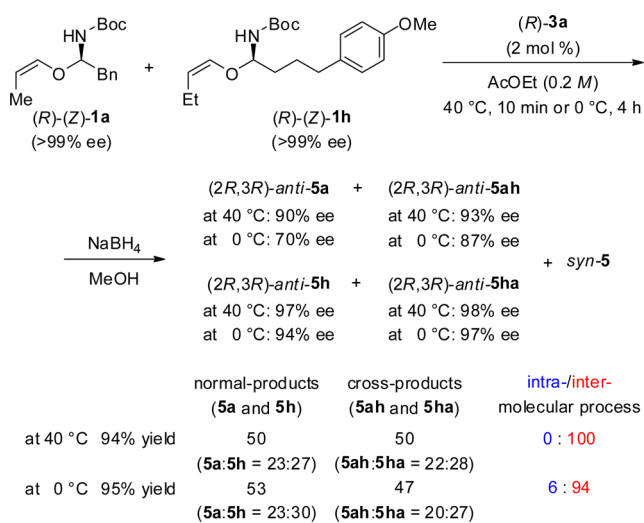
Scheme 4. Crossover Experiments of Enantiomerically Pure (S)-(Z)-1a and (S)-(Z)-1h



(Scheme 4 vs Scheme 3) because of the C–C matched combination. It should be pointed out that the intramolecular pathway tends to proceed in a retentive manner at the stereogenic center. In contrast, the cross-products, in particular **5ah**, displayed similar enantioselectivity to that observed in the reaction of racemic (Z)-1 (Scheme 4 vs Scheme 3). More importantly, the enantioselectivity of cross-product **5ah** was lower than that of normal-product **5a** (Scheme 4). The observed difference in enantioselectivity between **5ah** and **5a** implies that chiral information on substrate (Z)-1 is lost during the course of the intermolecular exchange process.

As mentioned above, it seems that the intermolecular exchange process is primarily responsible for the loss of chiral information on substrate (Z)-1. To validate this intriguing idea, we continued the crossover experiments using the C–C mismatched combination of (R)-(Z)-1 and (R)-3a. From the results of crossover experiments of racemic substrate (±)-(Z)-1 and C–C matched substrate (S)-(Z)-1, we surmised that the C–C mismatched combination undergoes the rearrangement through the intermolecular exchange process exclusively. With this in mind, crossover experiments of (R)-(Z)-1a and (R)-(Z)-1h were conducted under the same reaction conditions as those mentioned above. As shown in Scheme 5, indeed, the crossover reactions of (R)-(Z)-1a and **1h** proceeded smoothly to afford an approximately 1:1 mixture of normal- and cross-products. The estimated contribution of the intermolecular exchange process to the whole transformation was calculated to be 100% and 94% at 40 and 0 °C, respectively. It should be emphasized that at the high temperature of 40 °C, the rearrangement completely proceeded through the intermolecular exchange process. As pointed out previously, (Table 2, entries 2 and 5), enantiomerically pure substrate (R)-(Z)-1a predominantly underwent the rearrangement through the inversion at the stereogenic center and the inversion is the more dominant process at the higher temperature (Table 2, entry 2 vs entry 5). Together, the results strongly suggest that the inversion originates from the intermolecular exchange process, although catalyst (R)-3a promotes the inversion at the stereogenic center. In other words, the involvement of the intermolecular exchange process is the key to achieving the present enantioconvergent process.

Scheme 5. Crossover Experiments of Enantiomerically Pure (R)-(Z)-1a and (R)-(Z)-1h

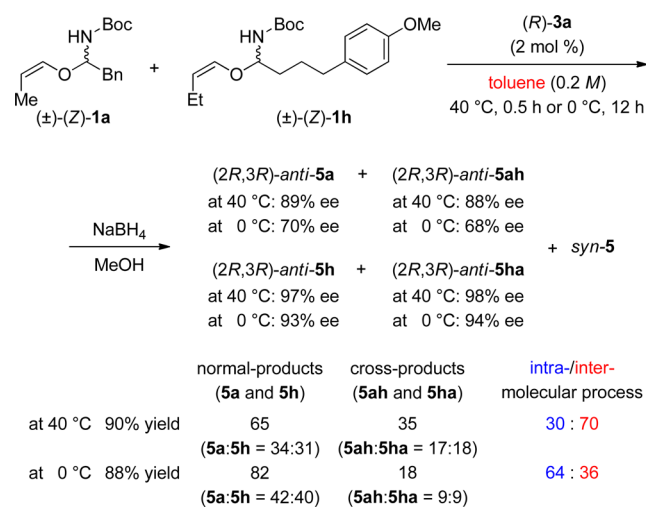


In contrast, at the low temperature of 0 °C, normal-product **5a** (0 °C: 70% ee) was obtained with low enantioselectivity compared with that obtained at the high temperature (40 °C: 90% ee). The low enantioselectivity of normal-product **5a** at the low temperature is rationalized by considering the fact that the intramolecular pathway proceeds in a retentive manner at the stereogenic center. The estimated percentage of the intramolecular pathway is 6% at 0 °C, and hence, normal-product **5a** was partially formed through the intramolecular pathway at that temperature. The participation of the intramolecular pathway, that is, the retentive process, leads to a considerable reduction of the enantioselectivity of normal-product **5a**. Furthermore, the origin of the anomalous temperature effect is also well rationalized on the basis of the participation of the intramolecular process, because the intramolecular pathway, that is, the retentive process, becomes dominant with decreasing reaction temperature.

As mentioned in the survey of our preliminary results, the present APF rearrangement is sensitive to the solvent employed. The solvents have a relatively basic nature; thus, ethyl acetate and acetone are more suitable for achieving high enantioselectivity than the less polar solvents, such as toluene and dichloromethane, despite the fact that these less polar solvents are commonly used in chiral phosphoric (Brønsted) acid-catalyzed reactions. On the basis of a series of the crossover experiments, it can be presumed that this intriguing solvent effect is caused from changes in rate of the intermolecular exchange process. Hence, we conducted the crossover experiments of racemic substrates (±)-(Z)-1a and (±)-(Z)-1h under the same conditions as those mentioned above with the exception of using the less polar solvent, toluene. In fact, as shown in Scheme 6 (vs Scheme 3), the rate of the intermolecular exchange process was markedly suppressed in toluene (in ethyl acetate → in toluene: 84% → 70% at 40 °C and 60% → 36% at 0 °C). In addition, the enantioselectivity of the product, in particular **5a** and **5ah**, was reduced as observed in our preliminary studies.^{8,37} It is obvious that the significant decrease in the enantioselectivities observed in toluene is primarily originated from the suppression of the intermolecular exchange process in the less polar solvent.

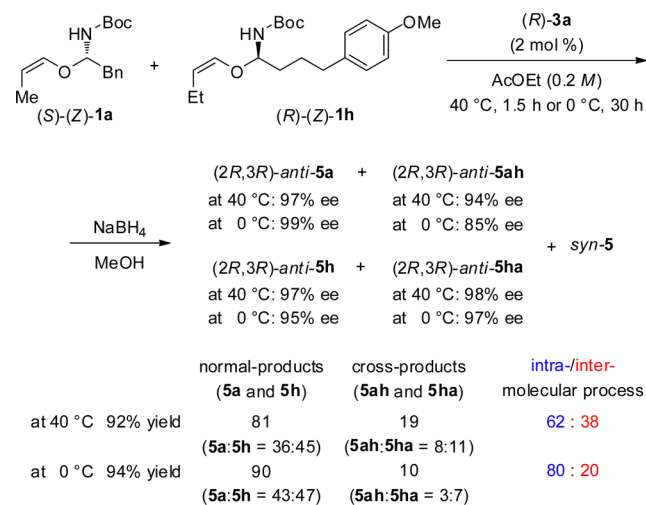
Finally, we attempted to perform crossover experiments of enantiomerically pure (S)-(Z)-1a and (R)-(Z)-1h having

Scheme 6. Crossover Experiments of Racemic (Z)-1a and (Z)-1h in Toluene



different absolute configurations from each other. The rearrangement rates of those substrates differed markedly and hence, it can be anticipated that the normal-products overwhelm the cross-ones. However, if the hemiaminal vinyl ether as it stands undergoes intermolecular exchange irrespective of the rearrangement, a considerable amount of cross-products would be formed by taking into consideration the previous crossover experiments. Crossover experiments of (S)-(Z)-1a and (R)-(Z)-1h were performed under the same reaction conditions as those mentioned above. As shown in Scheme 7, the formation of cross-products **5ah** and **5ha** was

Scheme 7. Crossover Experiments of Enantiomerically Pure (S)-(Z)-1a and (R)-(Z)-1h



significantly suppressed in this particular combination and hence, most of substrates (S)-(Z)-1a and (R)-(Z)-1h underwent the rearrangement independently. The results imply that the intermolecular exchange of the hemiaminal vinyl ethers without the formation of intermediates **A** and **B** may not be a plausible pathway for the exchange process.

CONCLUSION

The precise mechanism of the highly *anti*- and enantioselective aza-Petasis–Ferrier rearrangement of hemiaminal vinyl ethers catalyzed by a chiral phosphoric acid was investigated. In order to elucidate the mechanism of the present intriguing transformation, we conducted the following experiments: (A) X-ray crystallographic analysis of the recovered hemiaminal vinyl ether, (B) rearrangements of enantiomerically pure hemiaminal vinyl ethers, (C) theoretical studies on the transition states of the C–O bond cleavage and C–C bond formation steps, and (D) crossover experiments of two hemiaminal vinyl ethers having different vinyl ether and aliphatic substituents. The experimental results and the theoretical studies fully support the mechanistic proposal for the optical kinetic resolution, the enantioconvergent process, and the anomalous temperature effect observed in the present *anti*- and enantioselective APF rearrangement. The determination of the absolute configuration of the recovered hemiaminal vinyl ether by X-ray crystallographic analysis enabled to validate the stereochemical relationship between hemiaminal vinyl ethers and β -amino aldehydes as well as to evaluate theoretical studies on the C–O bond cleavage step of each enantiomer. The overall scheme of the present stereoselective APF rearrangement was proposed on the basis of experimental evidence from the rearrangements that used enantiomerically pure hemiaminal vinyl ethers and was well consistent with the energy profiles formulated by theoretical studies of the C–O bond cleavage and C–C bond formation steps. Indeed, the origin of the optical kinetic resolution of the racemic hemiaminal vinyl ether was clarified by theoretical studies on the C–O bond cleavage step. The formulated energy profiles coupled with observations from crossover experiments are beneficial to rationalize the enantioconvergent process in which racemic hemiaminal vinyl ethers are efficiently transformed into optically active β -amino aldehydes in the presence of a chiral phosphoric acid catalyst. Meanwhile, it became clear that the participation of intermolecular exchange is indispensable to achieving the present enantioconvergent process because the intermolecular exchange is responsible for the inversion at the initial stereogenic center of the hemiaminal vinyl ether. Furthermore, the experimental results of the rearrangements using enantiomerically pure hemiaminal vinyl ethers and the crossover experiments are also helpful to clarify the anomalous temperature effect, where the participation of the intramolecular pathway in the rearrangement is essential. The intramolecular pathway, that is, the retentive process, becomes dominant with decreasing reaction temperature and its involvement leads to a considerable decrease in enantioselectivity of the C–C mismatched transformation at the reduced temperature. We have elucidated the overall scheme of the present *anti*- and enantioselective APF rearrangement through detailed experimental and theoretical studies. The present method provides an efficient access to the highly *anti*- and enantioselective β -amino aldehydes having an aliphatic substituent at the β -position. Further studies on the application of the present activation mode of hemiaminal derivatives using chiral phosphoric acid catalysts are in progress with the aim of developing even more efficient enantioselective transformations.

ASSOCIATED CONTENT

Supporting Information

Representative experimental procedure, spectroscopic data for hemiaminal vinyl ethers (**1**), β -amino aldehydes (**2**), and amino alcohols (**5**), and determination of the absolute stereochemistry of **1g** and **5a**; complete list of authors in the Gaussian 09 reference; Cartesian coordinates and energies of stationary points and all transition structures. This material is available free of charge via the Internet at <http://pubs.acs.org>.

AUTHOR INFORMATION

Corresponding Author

mterada@m.tohoku.ac.jp

Present Address

[†]Department of Chemistry (Professor Johnston's group), Vanderbilt University, Nashville, TN 37235, United States.

Author Contributions

All authors have given approval to the final version of the manuscript.

Notes

The authors declare no competing financial interest.

ACKNOWLEDGMENTS

This work was partially supported by a Grant-in-Aid for Scientific Research on Innovative Areas "Advanced Molecular Transformations by Organocatalysts" from MEXT, Japan and NOVARTIS Foundation (Japan) for the Promotion of Science. We thank JSPS for a research fellowship for Young Scientists (Y.T.). We also sincerely thank Prof. T. Iwamoto and Prof. S. Ishida (Graduate School of Science, Tohoku University) for conducting X-ray analysis of (*Z*)-**1g** and Mitsubishi Chemical Co., Ltd. for supporting the HRMS analysis of new compounds and the HPLC analysis in the crossover experiments.

REFERENCES

- (1) For reviews, see: (a) Kobayashi, S.; Ishitani, H. *Chem. Rev.* **1999**, *99*, 1069–1094. (b) Liu, M.; Sibi, M. P. *Tetrahedron* **2002**, *58*, 7991–8035. (c) Córdova, A. *Acc. Chem. Res.* **2004**, *37*, 102–112. (d) Weiner, B.; Szymanski, W.; Janssen, D. B.; Minnaard, A. J.; Feringa, B. L. *Chem. Soc. Rev.* **2010**, *39*, 1656–1691. (e) Burns, N. Z.; Jacobsen, E. N. In *Science of Synthesis, Stereoselective Synthesis*; De Vries, J. G.; Molander, G. A.; Evans, P. A., Eds.; Georg Thieme Verlag KG: New York, 2011; Vol. 2, pp 785–834.
- (2) For recent reviews, see: (a) Ting, A.; Schaus, S. E. *Eur. J. Org. Chem.* **2007**, 5797–5815. (b) Verkade, J. M. M.; van Hemert, L. J. C.; Quaedflieg, P. J. L. M.; Rutjes, F. P. J. T. *Chem. Soc. Rev.* **2008**, *37*, 29–41. (c) Bhadury, P. S.; Song, B.-A. *Curr. Org. Chem.* **2010**, *14*, 1989–2006.
- (3) For *syn*-selective asymmetric Mannich reactions catalyzed by chiral amines, see: (a) Córdova, A.; Watanabe, S.; Tanaka, F.; Notz, W.; Barbas, C. F., III *J. Am. Chem. Soc.* **2002**, *124*, 1866–1867. (b) Hayashi, Y.; Tsuboi, W.; Ashimine, I.; Urushima, T.; Shoji, M.; Sakai, K. *Angew. Chem., Int. Ed.* **2003**, *42*, 3677–3680. (c) Notz, W.; Tanaka, F.; Watanabe, S.; Chowdari, N. S.; Turner, J. M.; Thayumanavan, R.; Barbas, C. F., III *J. Org. Chem.* **2003**, *68*, 9624–9634. (d) Córdova, A. *Chem.—Eur. J.* **2004**, *10*, 1987–1997. (e) Chowdari, N. S.; Suri, J. T.; Barbas, C. F., III *Org. Lett.* **2004**, *6*, 2507–2510. (f) Ibrahim, I.; Córdova, A. *Tetrahedron Lett.* **2005**, *46*, 2839–2843. (g) Fustero, S.; Jiménez, D.; Sanz-Cervera, J. F.; Sánchez-Roselló, M.; Esteban, E.; Simón-Fuentes, A. *Org. Lett.* **2005**, *7*, 3433–3436. (h) Hayashi, Y.; Urushima, T.; Shin, M.; Shoji, M. *Tetrahedron* **2005**, *61*, 11393–11404. (i) Cheong, P. H.-Y.; Zhang, H.; Thayumanavan, R.; Tanaka, F.; Houk, K. N.; Barbas, C. F., III *Org. Lett.* **2006**, *8*, 811–814.

- (4) For *anti*-selective asymmetric Mannich reactions catalyzed by chiral amines, see: (a) Córdova, A.; Barbas, C. F., III *Tetrahedron Lett.* **2002**, *43*, 7749–7752. (b) Kano, T.; Yamaguchi, Y.; Tokuda, O.; Maruoka, K. *J. Am. Chem. Soc.* **2005**, *127*, 16408–16409. (c) Franzén, J.; Marigo, M.; Fielenbach, D.; Wabnitz, T. C.; Kjærsgaard, A.; Jørgensen, K. A. *J. Am. Chem. Soc.* **2005**, *127*, 18296–18304. (d) Ibrahim, I.; Córdova, A. *Chem. Commun.* **2006**, 1760–1762. (e) Zhang, H.; Mitsumori, S.; Utsumi, N.; Imai, M.; Garcia-Delgado, N.; Mifsud, M.; Albertshofer, K.; Cheong, P. H.-Y.; Houk, K. N.; Tanaka, F.; Barbas, C. F., III *J. Am. Chem. Soc.* **2008**, *130*, 875–886. (f) Kano, T.; Hato, Y.; Yamamoto, A.; Maruoka, K. *Tetrahedron* **2008**, *64*, 1197–1203. (g) Pouliquen, M.; Blanchet, J.; Lasne, M.-C.; Rouden, J. *Org. Lett.* **2008**, *10*, 1029–1032. (h) Kano, T.; Yamaguchi, Y.; Maruoka, K. *Chem.—Eur. J.* **2009**, *15*, 6678–6687. (i) Gomez-Bengo, E.; Maestro, M.; Mielgo, A.; Otazo, I.; Palomo, C.; Velilla, I. *Chem.—Eur. J.* **2010**, *16*, 5333–5342.
- (5) Yang, J. W.; Stadler, M.; List, B. *Angew. Chem., Int. Ed.* **2007**, *46*, 609–611. List and co-workers demonstrated that proline can also catalyze the direct asymmetric Mannich reaction of acetaldehyde and *N*-Boc-protected imines to provide the simplest Mannich products as versatile chiral building blocks, albeit in low to moderate yields. See also: (a) Yang, J. W.; Chandler, C.; Stadler, M.; Kampen, D.; List, B. *Nature* **2008**, *452*, 453–455. *N*-benzoyl aldimines, see: (b) Hayashi, Y.; Okano, T.; Itoh, T.; Urushima, T.; Ishikawa, H.; Uchamaru, T. *Angew. Chem., Int. Ed.* **2008**, *47*, 9053–9058.
- (6) Vesely, J.; Rios, R.; Ibrahim, I.; Córdova, A. *Tetrahedron Lett.* **2007**, *48*, 421–425.
- (7) (a) Zhang, H.; Mitsumori, S.; Utsumi, N.; Imai, M.; Garcia-Delgado, N.; Mifsud, M.; Albertshofer, K.; Cheong, P. H.-Y.; Houk, K. N.; Tanaka, F.; Barbas, C. F., III *J. Am. Chem. Soc.* **2008**, *130*, 875–886. (b) Gianelli, C.; Sambri, L.; Carlone, A.; Bartoli, G.; Melchiorre, P. *Angew. Chem., Int. Ed.* **2008**, *47*, 8700–8702. (c) Dziejczak, P.; Schyman, P.; Kullberg, M.; Córdova, A. *Chem.—Eur. J.* **2009**, *15*, 4044–4048. (d) Kano, T.; Yamaguchi, Y.; Maruoka, K. *Angew. Chem., Int. Ed.* **2009**, *48*, 1838–1840. (e) Galzerano, P.; Agostino, D.; Bencivenni, G.; Sambri, L.; Bartoli, G.; Melchiorre, P. *Chem.—Eur. J.* **2010**, *16*, 6069–6076.
- (8) Terada, M.; Toda, Y. *J. Am. Chem. Soc.* **2009**, *131*, 6354–6355.
- (9) For reviews on metal complex/organocatalyst combined systems, see: (a) Park, Y. J.; Park, J.-W.; Jun, C.-H. *Acc. Chem. Res.* **2008**, *41*, 222–234. (b) Shao, Z.; Zhang, H. *Chem. Soc. Rev.* **2009**, *38*, 2745–2755. (c) Zhou, J. *Chem.—Asian J.* **2010**, *5*, 422–434. (d) Hashmi, A. S. K.; Hubbert, C. *Angew. Chem., Int. Ed.* **2010**, *49*, 1010–1012. (e) de Armas, P.; Tejedor, D.; García-Tellado, F. *Angew. Chem., Int. Ed.* **2010**, *49*, 1013–1016. (f) Zhong, C.; Shi, X. *Eur. J. Org. Chem.* **2010**, 2999–3025. (g) Rueping, M.; Koenigs, R. M.; Atodiresei, I. *Chem.—Eur. J.* **2010**, *16*, 9350–9365. (h) Lv, F.; Liu, S.; Hu, W. *Asian J. Org. Chem.* **2013**, *2*, 824–836.
- (10) Terada, M.; Machioka, K.; Sorimachi, K. *Angew. Chem., Int. Ed.* **2009**, *48*, 2553–2556.
- (11) For a review on organocatalytic rearrangements, see: Moyano, A.; El-Hamdouni, N.; Atlamsani, A. *Chem.—Eur. J.* **2010**, *16*, 5260–5273.
- (12) Frauenrath, H.; Arenz, T.; Raabe, G.; Zorn, M. *Angew. Chem., Int. Ed. Engl.* **1993**, *32*, 83–85.
- (13) Wille, A.; Tomm, S.; Frauenrath, H. *Synthesis* **1998**, 305–308.
- (14) Tayama, E.; Otoyama, S.; Isaka, W. *Chem. Commun.* **2008**, 4216–4218.
- (15) Koziol, A.; Grzeszczyk, B.; Koziol, A.; Staszewska-Krajewska, O.; Furman, B.; Chmielewski, M. *J. Org. Chem.* **2010**, *75*, 6990–6993.
- (16) For reviews on BINOL-derived phosphoric acids, see: (a) Terada, M. *Chem. Commun.* **2008**, 4097–4112. (b) Terada, M. *Synthesis* **2010**, 1929–1982. (c) Terada, M. *Bull. Chem. Soc. Jpn.* **2010**, *101*–119. (d) Zamfir, A.; Schenker, S.; Freund, M.; Tsogoeva, S. B. *Org. Biomol. Chem.* **2010**, *8*, 5262–5276. (e) Terada, M. *Curr. Org. Chem.* **2011**, *15*, 2227–2256. (f) Akiyama, T. In *Science of Synthesis, Asymmetric Organocatalysis 2, Brønsted Base and Acid Catalysts, and Additional Topics*; Maruoka, K., Ed.; Georg Thieme Verlag KG: New York, 2012; Vol. 2, pp169–217. (g) Terada, M.; Momiyama, N. In *Science of Synthesis, Asymmetric Organocatalysis 2, Brønsted Base and Acid Catalysts, and Additional Topics*; Maruoka, K., Ed.; Georg Thieme Verlag KG: New York, 2012; Vol. 2, pp219–296.
- (17) For seminal studies, see: (a) Akiyama, T.; Itoh, J.; Yokota, K.; Fuchibe, K. *Angew. Chem., Int. Ed.* **2004**, *43*, 1566–1568. (b) Uraguchi, D.; Terada, M. *J. Am. Chem. Soc.* **2004**, *126*, 5356–5357.
- (18) For reviews on chiral Brønsted acid catalysis, see: (a) Akiyama, T.; Itoh, J.; Fuchibe, K. *Adv. Synth. Catal.* **2006**, *348*, 999–1010. (b) Taylor, M. S.; Jacobsen, E. N. *Angew. Chem., Int. Ed.* **2006**, *45*, 1520–1543. (c) Doyle, A. G.; Jacobsen, E. N. *Chem. Rev.* **2007**, *107*, 5713–5743. (d) Akiyama, T. *Chem. Rev.* **2007**, *107*, 5744–5758. (e) Yamamoto, H.; Payette, N. In *Hydrogen Bonding in Organic Synthesis*; Pihko, P. M., Ed.; Wiley-VCH: Weinheim, 2009; pp 73–140. (f) Kampen, D.; Reisinger, C. M.; List, B. *Top. Curr. Chem.* **2010**, *291*, 395–456.
- (19) Mohr, J. T.; Ebner, D. C.; Stoltz, B. M. *Org. Biomol. Chem.* **2007**, *5*, 3571–3576.
- (20) For a seminal study of dynamic kinetic asymmetric transformation (DYKAT), see: (a) Trost, B. M.; Toste, F. D. *J. Am. Chem. Soc.* **1999**, *121*, 3543–3544. (b) Trost, B. M.; Bunt, R. C.; Lemoine, R. C.; Calkins, T. L. *J. Am. Chem. Soc.* **2000**, *122*, 5968–5976. See also: (c) Trost, B. M.; Fandrick, D. R. *Aldrichimica Acta* **2007**, *40*, 59–72. Selected examples of DYKAT, see: (d) Mohr, J. T.; Behenna, D. C.; Harned, A. M.; Stoltz, B. M. *Angew. Chem., Int. Ed.* **2005**, *44*, 6924–6927. (e) Roggen, M.; Carreira, E. M. *Angew. Chem., Int. Ed.* **2012**, *51*, 8652–8655. For direct enantio-convergent transformation (DET), see: (f) Ito, H.; Kuniti, S.; Sawamura, M. *Nat. Chem.* **2010**, *2*, 972–976.
- (21) For optical kinetic resolution of racemic substrates by chiral phosphoric acid catalysts, see: (a) Čorić, I.; Müller, S.; List, B. *J. Am. Chem. Soc.* **2010**, *132*, 17370–17373. (b) Guojian, L.; Birman, V. B. *Org. Lett.* **2011**, *13*, 356–358. (c) Wang, C.; Luo, H.-W.; Gong, L.-Z. *Synlett* **2011**, 992–994. (d) Mandai, H.; Murota, K.; Mitsudo, K.; Suga, S. *Org. Lett.* **2012**, *13*, 3486–3489. (e) Qabaja, G.; Wilent, J. E.; Benavides, A. R.; Bullard, G. E.; Petersen, K. S. *Org. Lett.* **2013**, *15*, 1266–1269. (f) Saito, K.; Shibata, Y.; Yamanaka, M.; Akiyama, T. *J. Am. Chem. Soc.* **2013**, *135*, 11740–11743. (g) Harada, S.; Kuwano, S.; Yamaoka, Y.; Yamada, K.; Takasu, K. *Angew. Chem., Int. Ed.* **2013**, *52*, 10227–10230.
- (22) Yamamoto, Y.; Kurihara, K.; Yamada, A.; Takahashi, M.; Takahashi, Y.; Miyaura, N. *Tetrahedron* **2003**, *59*, 537–542.
- (23) CCDC 985635 [(*S*)-(+)-(*Z*)-**1g**] contains the supplementary crystallographic data for this paper. This data can be obtained free of charge from The Cambridge Crystallographic Data Centre via www.ccdc.cam.ac.uk/data_request/cif.
- (24) Frisch, M. J. et al. *Gaussian 09*, Revision C.01; Gaussian, Inc.: Wallingford, CT, 2010.
- (25) Dapprich, S.; Komáromi, I.; Byun, K. S.; Morokuma, K.; Frisch, M. J. *J. Mol. Struct.: THEOCHEM* **1999**, *462*, 1–21.
- (26) (a) Becke, A. D. *J. Chem. Phys.* **1993**, *98*, 5648–5652. (b) Lee, C.; Yang, W.; Parr, R. G. *Phys. Rev. B* **1988**, *37*, 785–789.
- (27) For Gaussian basis sets: (a) Frisch, M. J.; Pople, J. A.; Binkley, J. S. *J. Chem. Phys.* **1984**, *80*, 3265–3269. (b) Hehre, W. J.; Radom, L.; Schleyer, P. v. R.; Pople, J. A. *Ab initio Molecular Orbital Theory*; John Wiley: New York, 1986, and references cited therein.
- (28) Head-Gordon, M.; Pople, J. A.; Frisch, M. J. *Chem. Phys. Lett.* **1998**, *153*, 503–506.
- (29) For diffuse function: Clark, T.; Chandrasekhar, J.; Spitznagel, G. W.; Schleyer, P. v. R. *J. Comput. Chem.* **1983**, *4*, 294–301.
- (30) Barone, V.; Cossi, M. *J. Phys. Chem. A* **1998**, *102*, 1995–2001.
- (31) For selected examples of theoretical studies on chiral phosphoric acid catalysis including two-point binding mode, see: (a) Yamanaka, M.; Itoh, J.; Fuchibe, K.; Akiyama, T. *J. Am. Chem. Soc.* **2007**, *129*, 6756–6764. (b) Yamanaka, M.; Hirata, T. *J. Org. Chem.* **2009**, *74*, 3266–3271. (c) Mori, K.; Katoh, T.; Suzuki, T.; Noji, T.; Yamanaka, M.; Akiyama, T. *Angew. Chem., Int. Ed.* **2009**, *48*, 9652–9654. (d) Marcelli, T.; Hammar, P.; Himo, F. *Chem.—Eur. J.* **2008**, *14*, 8562–8571. (e) Simón, L.; Goodman, J. M. *J. Am. Chem. Soc.* **2008**, *130*, 8741–8747. (f) Simón, L.; Goodman, J. M. *J. Am. Chem. Soc.* **2009**, *131*, 4070–4077. (g) Chen, X.-H.; Wei, Q.; Luo, S.-W.; Xiao,

H.; Gong, L.-Z. *J. Am. Chem. Soc.* **2009**, *131*, 13819–13825. (h) Li, N.; Chen, X.-H.; Song, J.; Luo, S.-W.; Fan, W.; Gong, L.-Z. *J. Am. Chem. Soc.* **2009**, *131*, 15301–15310. (i) Shi, F.-Q.; Song, B.-A. *Org. Biomol. Chem.* **2009**, *7*, 1292–1298. (j) Simón, L.; Goodman, J. M. *J. Org. Chem.* **2010**, *75*, 589–597. (k) Xu, S.; Wang, Z.; Li, Y.; Zhang, X.; Wang, H.; Ding, K. *Chem.—Eur. J.* **2010**, *16*, 3021–3035. (l) Cai, Q.-A.; Zheng, C.; You, S.-L. *Angew. Chem., Int. Ed.* **2010**, *49*, 8666–8669. (m) Simón, L.; Goodman, J. M. *J. Org. Chem.* **2011**, *76*, 1775–1788. (n) Shi, F.; Xing, G.-J.; Tao, Z.-L.; Luo, S.-W.; Tu, S.-J.; Gong, L.-Z. *J. Org. Chem.* **2012**, *77*, 6970–6979. (o) Mori, K.; Ichikawa, Y.; Kobayashi, M.; Shibata, Y.; Yamanaka, M.; Akiyama, T. *J. Am. Chem. Soc.* **2013**, *135*, 3964–3970. (p) Shibata, Y.; Yamanaka, M. *J. Org. Chem.* **2013**, *78*, 3731–3736.

(32) The *s-cis* conformation of $C=N-C=O(OT-Bu)$ is significantly stable to neglect the *s-trans* conformation. The orientation of the benzyl group is strictly restricted by the catalyst substituent introduced at the 3,3' positions of the binaphthyl backbone.

(33) Four transition states of (R)-(Z)-1a/(R)-3b, including $TS_{co,r1}$ and $TS_{co,r2}$, were obtained, whereas three transition states, including $TS_{co,s1}$ and $TS_{co,s2}$, were optimized for (S)-(Z)-1a/(R)-3b. See Supporting Information for details.

(34) $TS_{cc,re-syn}$ is also energetically unfavorable compared with $TS_{cc,re-anti}$ in terms of activation energy (Figure 11).

(35) Crossover experiments were also conducted by changing the concentrations of catalyst (R)-3a and racemic substrates (\pm)-(Z)-1a and 1h. However, no significant concentration effect was observed in all cases. See Supporting Information for details.

(36) A concerted pathway for the present rearrangement cannot be completely ruled out. However, the concerted mechanism may not be suitable for the major pathway of the present rearrangement because a considerable amount of cross-products was obtained even in the C—C matched combination, as shown in Scheme 4.

(37) The reactions of (\pm)-(Z)-1a catalyzed by (R)-3a were conducted in toluene at 40 and 0 °C to afford product 5a in 90% yield with 98% *anti* and 89% ee (for *anti*-5a) and in 84% yield with 97% *anti* and 68% ee (for *anti*-5a), respectively.